Engineered Science
DOI: https://dx.doi.org/10.30919/es1616

# Unraveling the Role of Functional Groups in Polyaniline for $NH_3$ Sensing: A Theoretical Approach

Areyi Nulima,[1] Anuar Aldongarov,[2] Saniya Sarsenova,[3] Aigerim Ibrayeva[4,*] and Mirat Karibayev[5,6,*]

## Abstract

One of the pressing challenges in the hydrogen energy field is the safe storage and transport of hydrogen, where leakage can pose severe risks, making the detection of hydrogen and its carriers, such as ammonia, critically important. Polyaniline (PANI), due to its tunable conductivity and chemical reactivity, has emerged as a promising material for ammonia sensing applications. This study investigates the interaction of ammonia with unfunctionalized oligomeric PANI and its functionalized derivatives ($NH_2$- and OH-functionalized PANI) to evaluate their relative gas-sensing performance using Density Functional Theory and classical Molecular Dynamics simulations. Based on literature, $NH_3$ sensitivity is hypothesized to follow the trend: $NH_2$-functionalized PANI > OH-functionalized PANI > unfunctionalized PANI. Optimized geometries revealed increased reactivity and altered charge distributions due to functionalization. Molecular electrostatic potential maps and Mulliken charge analysis showed that $NH_2$ and OH groups enhance local electron density near hydrogen bonding sites, promoting stronger $NH_3$ interactions. Reduced density gradient and non-covalent interaction plots confirmed enhanced hydrogen bonding and van der Waals interactions, especially for $NH_2$-functionalized PANI. Quantum Theory of Atoms in Molecules analysis revealed more and denser bond critical points for $NH_2$-functionalized PANI. Interaction energy calculations further supported this trend. These findings provide molecular insights for designing highly selective and sensitive PANI-based ammonia sensors.

*Keywords:* Hydrogen carrier; Ammonia; Sensor; Polyaniline; Selectivity; Density functional theory; Classical all-atom molecular dynamics.
Received: 15 May 2025; Revised: 12 June 2025; Accepted: 03 July 2025.
Article type: Research article.

## 1. Introduction

Ammonia ($NH_3$), a colorless and corrosive gas with a sharp odor, is commonly used across various industrial and agricultural applications. As a hydrogen carrier in transportation systems, it poses a risk of leakage, which necessitates effective detection and monitoring. It is primarily released through fertilizer applications, livestock waste, the chemical industry, and textile manufacturing, with additional contributions from domestic sources.[1-3] Despite its critical role in these applications, $NH_3$ is a significant environmental pollutant and poses serious health risks upon exposure. Even at low concentrations, $NH_3$ can cause irritation to the eyes, nose, and throat, while prolonged or high-level exposure may lead to severe respiratory damage, including pulmonary edema and permanent blindness. Due to its toxicity and volatility, there is a compelling need for real-time, sensitive detection systems capable of operating in varied environmental conditions.

The human olfactory system can detect ammonia at approximately 25 ppm; however, for effective industrial and environmental monitoring, sensors with sub-ppm or even ppb-level sensitivity are required.[4-7] Conventional $NH_3$ sensors based on metal oxide semiconductors (*e.g.,* $SnO_2$, ZnO, and $WO_3$) offer acceptable sensitivity but are often hindered by high operating temperatures, poor selectivity, and long-term instability. These drawbacks limit their practical use, particularly in settings that demand low-power operation, ambient-temperature response, and long-term durability. Therefore, researchers have increasingly turned to organic sensing materials, particularly conducting polymers as viable alternatives. Among conducting polymers, polyaniline (PANI) has emerged as a highly promising candidate for gas sensing applications. PANI exhibits desirable features such as high

[1]*Department of Mathematics, School of Sciences and Humanities, Nazarbayev University, 53 Kabanbay Batyr avenue, Astana, 010000, Kazakhstan*
[2]*Department of Technical Physics, L. N. Gumilyov Eurasian National University, Satpayev 2, Astana, 010000, Kazakhstan*
[3]*Higher School of Law, Astana International University, 8 Kabanbay Batyr avenue, Astana, 020000, Kazakhstan*

**Table 1:** Overview of recent studies on PANI-Based Ammonia Sensing

| Study Focus | Methodology | Key Findings |
|---|---|---|
| HCl-doped PANI sensing[21,22] | MD simulations | $NH_3$ interacts preferentially with $Cl^-$ dopants (3.1 Å). Density and diffusion match experiments. |
| DFT-based PANI models[23] | Non-equilibrium DFT | Multi-chain models exhibit resistance shifts consistent with sensing at 3-12 ppm $NH_3$ concentrations. |
| Ag/Cu-PANI composites[24] | Experimental synthesis | Enhanced $NH_3$ sensitivity via improved electron transport in hybrid nanostructures. |
| PANI/ZnO heterostructures[25] | Experimental testing | High sensitivity due to interfacial charge transfer effects between PANI and ZnO. |

electrical conductivity, ease of synthesis, environmental and tunable surface chemistry. These properties make PANI a cost-effective and flexible material for integration into $NH_3$ sensors.[8-12] Its gas sensing capability is primarily based on changes in its electrical conductivity when exposed to $NH_3$ molecules. These changes arise due to acid–base interactions between the electron-donating $NH_3$ and the protonated sites on PANI chains, leading to a reduction in charge carriers and, consequently, a measurable increase in resistance.

Conducting polymers such as PANI have garnered significant interest in gas-sensing applications due to their tunable electrical conductivity, chemical stability, and ease of functionalization. Among various target gases, $NH_3$, nitrogen dioxide, carbon monoxide, and hydrogen sulfide are commonly studied for their environmental and industrial relevance. PANI demonstrates particularly high sensitivity to $NH_3$, attributed to acid–base interactions between $NH_3$'s lone pair electrons and the protonated imine sites along the PANI backbone, resulting in measurable conductivity changes. In contrast, oxidizing gases like nitrogen dioxide interact with PANI through charge transfer and redox reactions, often yielding stronger but less reversible responses.[13-15] Carbon monoxide and hydrogen sulfide typically exhibit weaker interactions, necessitating further material modifications for effective detection. Given $NH_3$'s widespread presence and the relatively reversible nature of its interaction with PANI, this study focuses on exploring its sensing behavior using both unfunctionalized and functionalized PANI oligomers, offering insight for broader gas sensor design strategies.

To further enhance sensing performance, composite and hybrid materials based on PANI have been explored. Functionalizing PANI with metal nanoparticles, metal oxides, or other chemical groups improves its sensitivity, selectivity, transfer pathways.[16-20] However, despite these advances, and stability by tailoring its surface energy and electron understanding the fundamental molecular-level interactions between PANI and ammonia remains an area of active research, especially with regard to the influence of chemical functionalization.

To better contextualize recent advances in this field, Table 1 summarizes key findings from recent experimental and computational studies related to PANI-based ammonia sensing.

These studies illustrate how both theoretical and experimental approaches have deepened our understanding of PANI's $NH_3$ sensing mechanisms. Molecular level modeling, such as density functional theory (DFT) and classical all-atom molecular dynamics (MD) simulations, has proven to be a valuable complement to experimental methods by elucidating the electronic structure, charge transfer behavior, and binding interactions in sensor materials.

Building on these insights, the present study investigates the atomistic interactions between $NH_3$ molecules and functionalized PANI chains using a combination of DFT and classical all-atom MD simulations. Specifically, computational models were constructed for dimers of non-functionalized PANI, $NH_2$-functionalized PANI, and OH-functionalized PANI. These systems were evaluated in both the presence and absence of $NH_3$ to determine the influence of chemical functionalization on sensing performance. The choice of amino and hydroxyl functional groups was motivated by their electron-donating nature, which is expected to influence hydrogen bonding and charge transfer processes with $NH_3$.

Our integrated computational approach provides a detailed understanding of structural, energetic, and dynamic aspects of $NH_3$ sensing at the molecular scale. By comparing functionalized and pristine PANI systems, we aim to identify key molecular descriptors such as binding energy, interaction distance, and hydrogen bonding patterns that govern the sensitivity of PANI-based sensors. These results offer valuable guidance for the rational design of next-generation polymer-based gas sensors with improved performance and robustness.

Despite significant interest in PANI-based materials for gas sensing, there remains a lack of detailed molecular-level understanding of how functionalization influences their interaction with $NH_3$, particularly in terms of electronic and structural properties. To address this gap, we employed a

[4]*Higher School of Social Sciences and Humanities, Astana International University, 8 Kabanbay Batyr avenue, Astana, 020000, Kazakhstan*
[5]*Department of Chemical and Materials Engineering, School of Engineering and Digital Sciences, Nazarbayev University, 53 Kabanbay Batyr avenue, Astana, 010000, Kazakhstan*
[6]*Laboratory of Renewable Energy, National Laboratory Astana, Nazarbayev University, 53 Kabanbay Batyr avenue, Astana, 010000, Kazakhstan*
**E-mail :* aigerimibrayeva7@gmail.com (A. I);
mirat.karibayev@nu.edu.kz (M. K)

combined computational approach using DFT and classical all-atom MD simulations to investigate the interactions between $NH_3$ and three PANI oligomers: unfunctionalized PANI, $NH_2$-functionalized PANI, and OH-functionalized PANI. This study aims to elucidate how functional groups affect $NH_3$ sensing performance at the atomic level. The paper is organized as follows: (i) section 2 presents the computational methodologies; (ii) section 3 discusses the quantum chemical and structural results; and (iii) section 4 concludes with key findings and implications for sensor design.

## 2. Methodology

### 2.1 System of interest

These models were designed based on established experimental data to ensure relevance to real-world synthesized materials. The choice of $NH_2$ and OH functional groups reflect their potential to enhance interaction with $NH_3$ through hydrogen bonding and electronic effects. By examining structural and electronic changes induced by $NH_3$ adsorption, this approach enables atomistic-level insight into the sensing mechanism. The combination of DFT and classical all-atom MD allows for a detailed evaluation of adsorption behavior, interaction energies, and conformational stability, contributing to the rational design of high-performance PANI-based ammonia sensors.

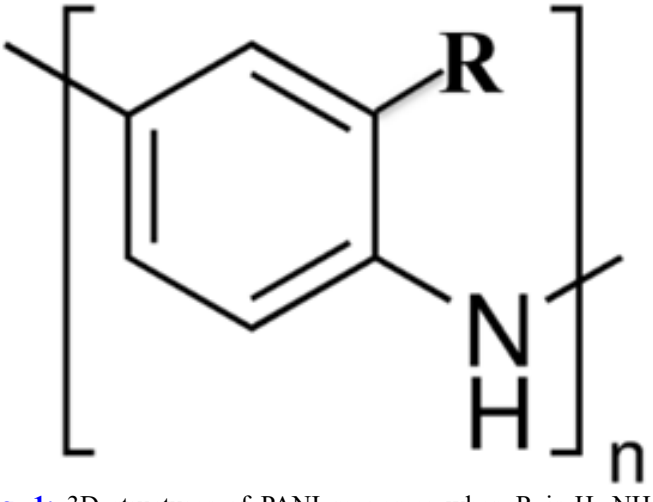


**Fig. 1:** 3D structures of PANI monomer when R is H, $NH_2$-functionalized PANI monomer when R is $NH_2$, and (c) OH-functionalized PANI monomer when R is OH.

To investigate the $NH_3$ sensing PANI, computational models were developed using DFT calculations and classical all-atom MD simulations. The models consisted of dimers of non-functionalized PANI, $NH_2$-functionalized PANI, and OH-functionalized PANI, which were evaluated as sensor materials in the presence and absence of $NH_3$ gas (Fig. 1). These computational models were designed based on prior experimental studies, ensuring consistency with established synthesis and characterization methodologies. By leveraging insights from both experimental and theoretical research, this approach provides a comprehensive understanding of $NH_3$ gas detection at the molecular level.

### 2.2 DFT calculations

DFT calculations were carried out to investigate the ground-state electronic structures of functionalized PANI dimers in both $NH_3$-free and $NH_3$-adsorbed configurations. Key quantum chemical descriptors derived from these calculations include optimized geometries, molecular electrostatic potential (MEP) maps, Mulliken charge distributions, reduced density gradient (RDG) analysis, non-covalent interaction (NCI) plots, and critical point (CP) identification. These analyses provide essential insights into the adsorption behavior and intermolecular interactions that govern $NH_3$ sensing performance.

The B3LYP hybrid functional was employed due to its proven reliability in predicting molecular geometries and electronic properties.[26] The 6-311++G(2d,p) basis set was selected to ensure an optimal balance between computational efficiency and accuracy in electron density descriptions.[27] Geometry optimizations were conducted for both isolated and $NH_3$-interacting PANI systems to assess structural and electronic changes upon gas adsorption.

All DFT computations were performed using the GAUSSIAN16 software suite.[28] Post-processing analyses utilized GaussView (v6.0) for visualization,[29] Multiwfn for detailed wavefunction evaluation, and VMD for graphical representation.[30-32] These computational tools enabled a comprehensive understanding of the adsorption mechanisms and electronic responses of functionalized PANI systems toward $NH_3$ molecules.

### 2.3 Classical all-atom MD simulations

The goal was to assess the adsorption behavior and interaction dynamics of $NH_3$ in the presence of PANI, $NH_2$-functionalized PANI, and OH-functionalized PANI oligomers, each composed of ten repeat units. These molecular structures were constructed based on topology files and force field parameters obtained from the Automated Topology Builder (ATB),[33] employing the GROMOS 54a7 force field.[34]

The simulation setup involved placing each PANI system into a $10 \times 10 \times 10$ nm³ cubic box filled with air components ($N_2$ and $O_2$) and a controlled number of $NH_3$ gas molecules.

The specific composition of each system is detailed in Table 2. $NH_3$ was introduced alongside air molecules to realistically simulate ambient conditions, with each simulation containing 15,522 $N_2$ molecules, 4,378 $O_2$ molecules, and 100 $NH_3$ molecules.

Initial energy minimization was performed using the steepest descent algorithm until the maximum force fell below 1000 kJ/mol/nm. Following minimization, two equilibration phases were conducted: a 0.1 ns simulation under the NVT ensemble at 298 K to stabilize temperature, followed by a 0.1 ns NPT run at 298 K and 1 bar to achieve pressure equilibration. Production simulations were then carried out for

**Table 2:** Description of classical all-atom MD simulation settings.

| Description | $N_2$ | $O_2$ | $H_2$ | Polymer |
|---|---|---|---|---|
| PANI in the presence of $NH_3$ gas and air | 15522 | 4378 | 100 | 10 |
| $NH_2$ functionalized PANI in the presence of $NH_3$ gas | 15522 | 4378 | 100 | 10 |
| OH functionalized PANI in the presence of $NH_3$ gas | 15522 | 4378 | 100 | 10 |

30 ns to evaluate ammonia diffusion, adsorption characteristics, and polymer–gas interaction behavior.

Short-range interactions were treated with a 1.0 nm cutoff, and long-range electrostatics were managed using the Particle Mesh Ewald (PME) method with a grid spacing of 0.16 nm. All bond lengths involving hydrogen atoms were constrained using the LINCS algorithm.[35] Temperature was controlled using the Nose–Hoover thermostat,[36] while the Berendsen barostat[37] maintained pressure throughout the simulations. Periodic boundary conditions were applied in all directions to emulate bulk-phase behavior and eliminate surface effects.

Classical all-atom MD simulations were conducted using the GROMACS 2018.1 package to explore the atomistic interactions between $NH_3$ and PANI systems, including both non-functionalized and functionalized variants.[38] The equilibrated density of the simulation system was approximately 1.168 kg/m³, which is close to the density of air under ambient conditions, confirming proper equilibration of the gas-phase system.[39]

## 3. Results and discussion

### 3.1 Optimized structures

Fig. 2 presents the optimized geometries of unfunctionalized PANI, $NH_2$ -functionalized PANI, and OH-functionalized PANI in the presence of $NH_3$. The focus is on evaluating structural parameters, namely hydrogen bond distances and bond angles, to understand how functional groups modulate $NH_3$ interaction, thus impacting sensing efficiency.

In the unfunctionalized PANI, $NH_3$ interacts primarily with the protonated imine nitrogen ($N^+$–H), forming a strong hydrogen bond with a bond length of 2.04 Å and bond angle of 169.27°. This interaction facilitates the reversible proton transfer that converts $NH_3$ to ammonium ($NH_4^+$), resulting in a reduction in the number of polarons and decreased conductivity. However, the absence of additional electron-donating groups limits the strength and multiplicity of interactions.

Upon OH functionalization, the interaction distance slightly increases to 2.05 Å, with a nearly linear hydrogen bond angle of 175.66°, indicating enhanced directional hydrogen bonding. The hydroxyl group acts as both hydrogen bond donor and acceptor, contributing to localized charge redistribution. Yet, the OH group's relatively lower electron-donating strength compared to $NH_2$ results in only moderate improvement in $NH_3$ binding.

The $NH_2$-functionalized PANI demonstrates a weaker geometric hydrogen bond (2.71 Å, 132.50°), but this is compensated by stronger electronic effects. The amino group significantly increases the local electron density around the adsorption site, enhancing charge transfer with $NH_3$ even if the bond geometry is less ideal. This suggests that $NH_2$ groups facilitate stronger overall interactions through electronic stabilization rather than just geometry, which aligns with the highest observed sensing efficiency.

These findings support the hypothesized trend: $NH_2$-functionalized PANI > OH-functionalized PANI > unfunctionalized PANI. Functional groups not only influence hydrogen bonding geometries but also modulate local electronic environments critical for reversible protonation and efficient electron injection upon $NH_3$ exposure.

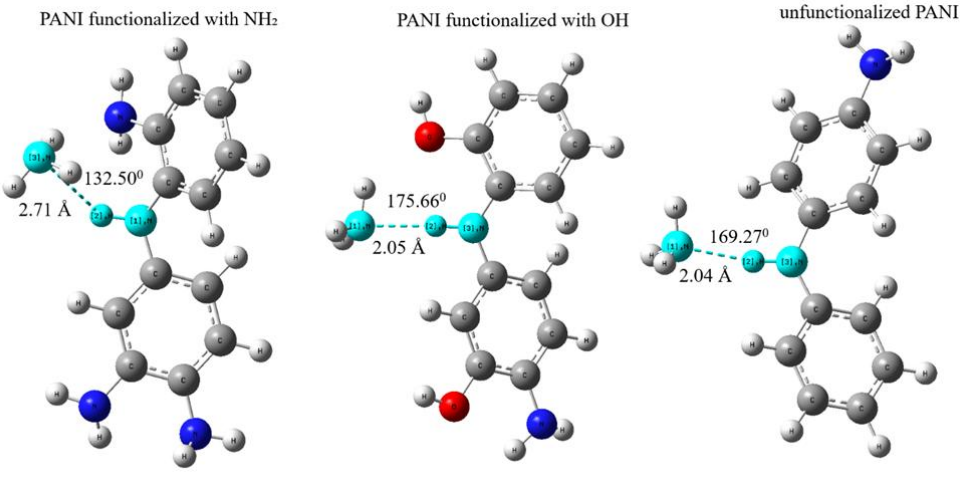


**Fig. 2:** Optimized structures of PANI functionalized with $NH_2$, PANI functionalized with OH, and unfunctionalized PANI in the presence of $NH_3$ Color key: white (H atom); grey (C atom); blue (N atom); red (O atom).

### 3.2 Molecular electrostatic potential maps

Fig. 3 presents the MEP maps for $NH_2$-functionalized PANI, OH-functionalized PANI, and unfunctionalized PANI, all in the presence of adsorbed $NH_3$ MEP maps are powerful tools for visualizing the charge distribution of a molecule, where red regions indicate areas of high electron density (electronegative potential), and blue regions represent areas of low electron density (electropositive potential). These maps are crucial for understanding preferred sites for nucleophilic and electrophilic attack and, in the context of gas sensing, the strength and nature of interactions with target analytes.

For $NH_2$-functionalized PANI complexed with $NH_3$, the MEP map strikingly reveals a distinct red region around the nitrogen atoms of the functionalizing amine group and the adsorbed $NH_3$. This high electron density suggests a strong localized negative potential, indicative of electron-rich sites. The adjacent blue regions, particularly those associated with the hydrogen atoms of $NH_3$ and the PANI backbone, point to electron-deficient areas. This clear spatial differentiation, with a prominent red region near the interaction site, strongly supports the formation of robust interactions, likely involving hydrogen bonding and potentially some degree of charge transfer from the electron-donating $NH_3$ to the PANI system. The strong electrostatic attraction facilitated by these distinct potential differences would enhance the binding affinity and, consequently, the sensing response.

In contrast, the MEP map for OH-functionalized PANI with $NH_3$ shows a less pronounced and more diffuse red region around the hydroxyl groups compared to the amino group in the $NH_2$-PANI system. While the hydroxyl group is also electron-rich, its potential distribution appears less concentrated or as extensively interacting with the adsorbed $NH_3$. Similarly, the unfunctionalized PANI in the presence of $NH_3$ exhibits even more diffuse and less distinct electrostatic potential variations at the interaction interface. The red regions are more spread out, and the blue regions are less intense, suggesting weaker, less specific electrostatic interactions between the PANI backbone and the $NH_3$ molecule.

These MEP map observations directly support our hypothesis regarding the superior $NH_3$ sensitivity of $NH_2$-functionalized PANI. The more pronounced and localized electron-rich regions (red) around the amino functional group create an optimal electrostatic environment for attracting and binding the electron-donating $NH_3$ molecule. This enhanced electrostatic interaction, as visualized by the MEP maps, translates to a more effective and detectable sensing mechanism compared to the less favorable interactions seen with OH-functionalized and unfunctionalized PANI.

### 3.3 Mulliken charge analysis

Fig. 4 illustrates the Mulliken charge distributions for $NH_2$-functionalized PANI, OH-functionalized PANI, and unfunctionalized PANI, all interacting with adsorbed ammonia. Mulliken charges provide a quantitative measure of the partial atomic charges within a molecule, indicating the distribution of electron density among the constituent atoms. Red regions indicate a higher electron density (more negative charge), while green regions signify lower electron density (more positive charge). These charges are particularly insightful for assessing charge transfer phenomena during molecular interactions, which are paramount in gas sensing.

For the $NH_2$-functionalized PANI system with adsorbed $NH_3$, a distinct red hue is observed around the nitrogen atom of the $NH_2$ functional group and the nitrogen atom of the adsorbed $NH_3$ molecule, signifying a higher electron density. Conversely, the hydrogen atoms, particularly those involved in potential hydrogen bonding with the PANI backbone, tend to be more green, indicating a partial positive charge.

This pattern suggests a clear charge redistribution within the complex, where the electron-donating $NH_3$ molecule

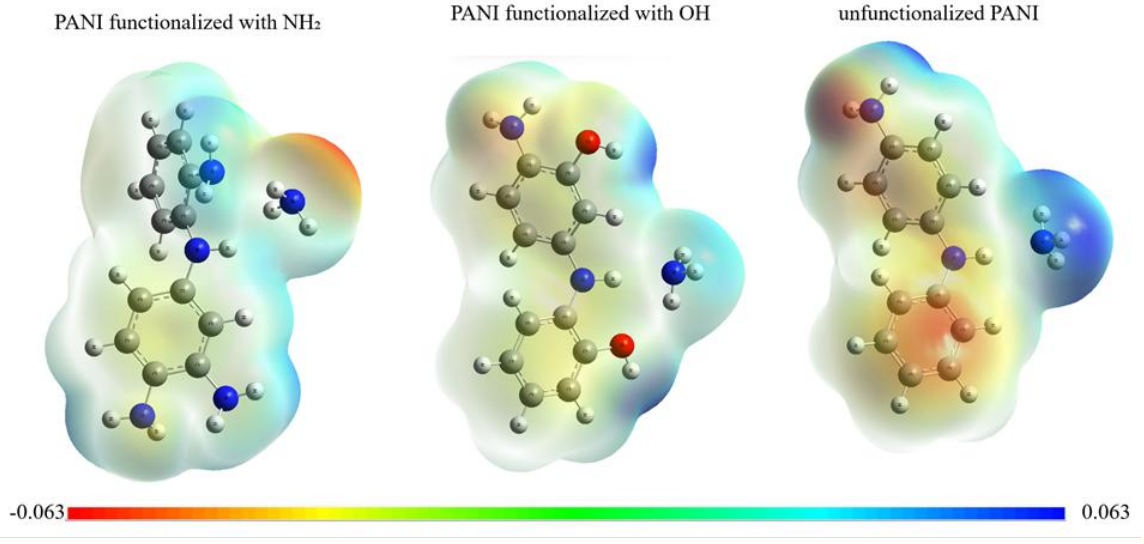


**Fig. 3:** MEP maps of PANI functionalized with $NH_2$, PANI functionalized with OH, and unfunctionalized PANI in the presence of $NH_3$. Color key: white (H atom); grey (C atom); blue (N atom); red (O atom).

facilitates a transfer of electron density, likely from the $NH_3$ to the functionalized PANI. The localized negative charges on the nitrogen centers indicate areas that are highly receptive to the $NH_3$ electrons, suggesting a strong and favorable interaction. This substantial charge transfer upon $NH_3$ adsorption is a key factor contributing to a detectable change in the electronic properties of the material, enhancing its sensing capabilities.

In contrast, the Mulliken charge distribution for OH-functionalized PANI interacting with $NH_3$ shows a less pronounced and more diffuse electron density accumulation around the oxygen atom of the hydroxyl group. While oxygen is electronegative, the extent of charge localization and transfer appears to be less significant than in the amino-functionalized system. The regions of electron enrichment (red) are not as intense or widespread. Similarly, the unfunctionalized PANI, when interacting with $NH_3$, displays even more diffuse and less distinct charge variations across its atoms. The overall charge redistribution appears minimal, suggesting a weaker and less specific interaction with the $NH_3$ molecule.

These observations from the Mulliken charge analysis strongly corroborate our hypothesis. The ability of the $NH_2$ functional group to facilitate a more significant and localized charge transfer from the adsorbed $NH_3$ molecule to the PANI backbone explains the superior $NH_3$ sensitivity of $NH_2$-functionalized PANI. This pronounced charge transfer leads to larger changes in the material's conductivity or other measurable electrical properties, which are critical for effective gas detection, outperforming the less effective interactions observed in OH-functionalized and unfunctionalized PANI.

### 3.4 Reduced density gradient

Fig. 5 presents the RDG plots for (a) unfunctionalized PANI, (b) $NH_2$-functionalized PANI, and (c) OH-functionalized PANI, all in the presence of $NH_3$. RDG analysis is a valuable computational tool that reveals regions of non-covalent interactions by mapping electron density and its gradients. In these plots, low RDG values indicate zones where non-covalent interactions are pronounced, while the sign of the second eigenvalue of the electron density Hessian (sign($\lambda_2$)) differentiates between attractive interactions (negative sign, such as hydrogen bonding) and repulsive ones (positive sign, like steric hindrance).

In the case of unfunctionalized PANI with $NH_3$, the RDG plot highlights weak hydrogen bonding between the polymer backbone and $NH_3$. These interactions, although not as strong as those involving functional groups, still contribute to ammonia's detectable affinity to the PANI surface. Slight peaks in the attractive region suggest van der Waals and weak hydrogen bond formation.

For $NH_2$-functionalized PANI, the RDG plot changes significantly. The $NH_2$ group offers a favorable site for hydrogen bonding with $NH_3$ due to the lone pair on nitrogen and available hydrogen atoms. This results in pronounced peaks in the negative sign ($\lambda_2$) region, indicating strong attractive interactions. The RDG isosurface may appear more structured, revealing spatially localized interaction zones.

In OH-functionalized PANI, the RDG plot also displays strong hydrogen bonding interactions, likely more intense or numerous depending on molecular orientation.

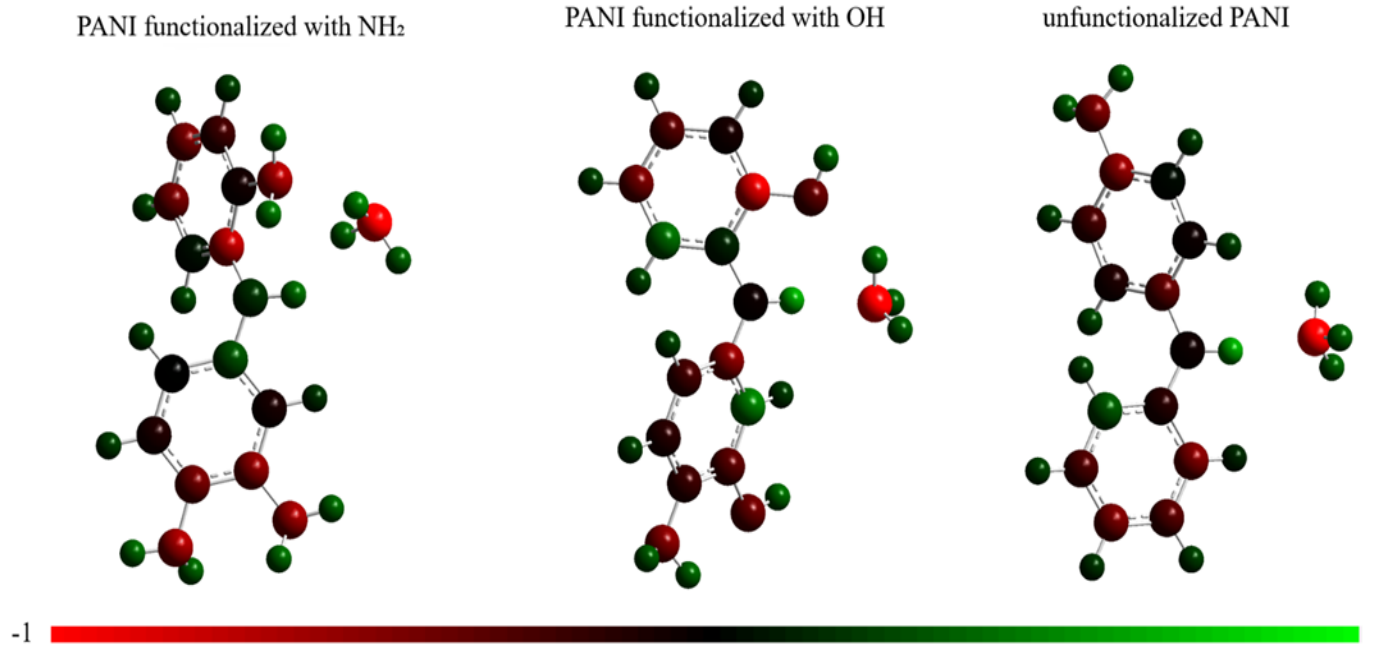


**Fig. 4:** Mulliken charges of PANI functionalized with $NH_2$, PANI functionalized with OH, and unfunctionalized PANI in the presence of $NH_3$. Color key: white (H atom); grey (C atom); blue (N atom); red (O atom).

The OH group, being both a donor and acceptor, engages robustly with $NH_3$, evident through broadened and intensified RDG features in the attractive region.

Comparison across the three cases reveals how functionalization significantly enhances PANI's interaction with $NH_3$. These findings underscore the importance of specific functional groups in tailoring PANI's sensitivity and selectivity for gas sensing. The RDG analysis in Fig. 5 visually reinforces the role of non-covalent interactions, especially hydrogen bonding, in driving the ammonia detection capabilities of functionalized PANI systems.

### 3.5 Non-Covalent Interactions

Fig. 6 illustrates the NCI plots for $NH_2$-functionalized PANI, OH-functionalized PANI, and unfunctionalized PANI, all in the presence of adsorbed $NH_3$. NCI plots are a powerful visualization tool derived from electron density and its derivatives, enabling the identification and characterization of various non-covalent interactions, including hydrogen bonds, van der Waals forces, and steric repulsions. In these plots, green regions typically indicate weak attractive interactions (like van der Waals forces), blue regions denote strong attractive interactions (such as hydrogen bonds), and red regions highlight strong repulsive interactions (steric clashes).

For the $NH_2$-functionalized PANI system complexed with $NH_3$, the NCI plot reveals prominent blue isosurfaces located between the hydrogen atoms of the adsorbed $NH_3$ and the nitrogen atoms of both the PANI backbone and the amino functional group. These blue regions are a clear indication of strong attractive interactions, characteristic of hydrogen bonding. Furthermore, green isosurfaces are observed, suggesting the presence of additional weak attractive interactions, likely van der Waals forces, contributing to the overall stability of the complex. The presence of these distinct blue regions underscores the formation of specific and robust hydrogen bonds, facilitating a strong binding of $NH_3$ to the functionalized PANI. This strong non-covalent interaction is a direct contributor to the enhanced sensitivity of $NH_2$-functionalized PANI towards $NH_3$.

In contrast, the NCI plot for OH-functionalized PANI interacting with $NH_3$ shows relatively smaller and less extensive blue regions around the hydroxyl groups compared to the amino-functionalized system. While some hydrogen bonding might occur, the interactions appear less significant and more diffuse. The green regions, indicating van der Waals interactions, are also present but do not suggest a dominant attractive force. Similarly, for the unfunctionalized PANI interacting with $NH_3$, the NCI plot displays very sparse and weak attractive interactions. The blue regions are almost absent, and the green regions are minimal, indicating that $NH_3$ interacts primarily through very weak van der Waals forces with the unfunctionalized PANI backbone.

These NCI plot analyses provide compelling visual evidence to support our hypothesis that $NH_2$-functionalized PANI exhibits superior $NH_3$ sensitivity. The formation of strong, directional hydrogen bonds, clearly visualized by the blue isosurfaces in the NCI plot, plays a critical role in anchoring the $NH_3$ molecule to the sensing material. This enhanced non-covalent interaction allows for a more effective and stable adsorption of $NH_3$, leading to a more significant and detectable change in the electronic properties of the $NH_2$-functionalized PANI, thereby improving its sensing performance compared to the other less interactive PANI derivatives.

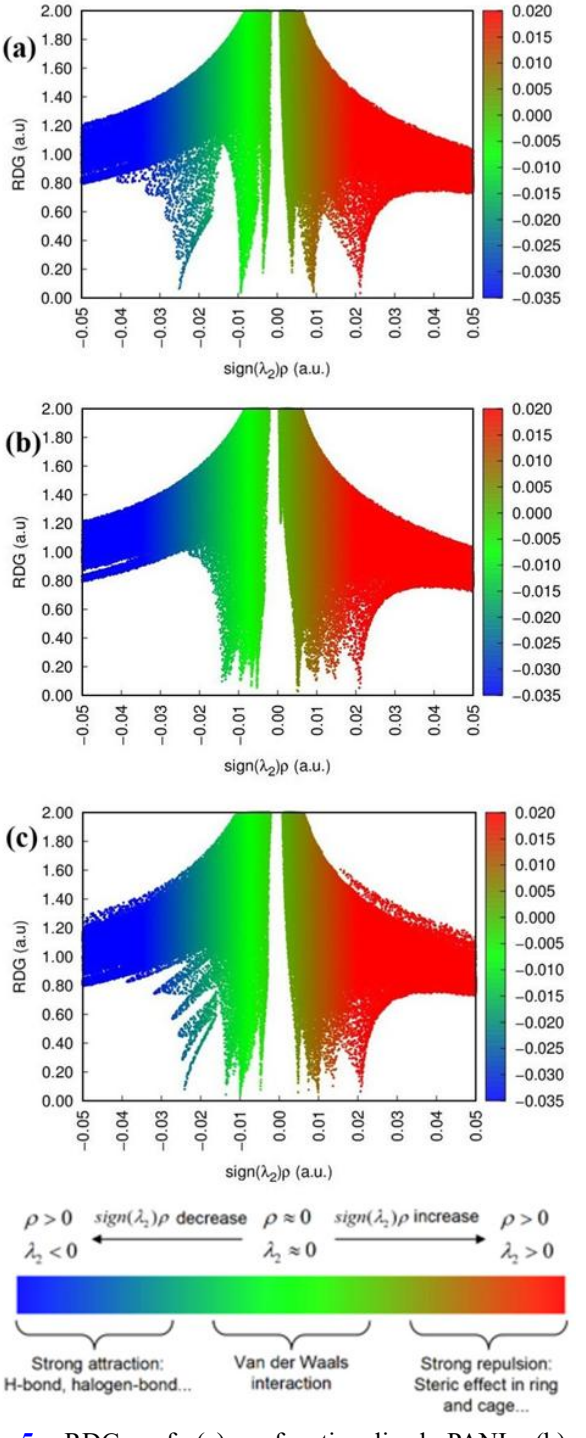


**Fig. 5:** RDGs of (a) unfunctionalized PANI, (b) PANI functionalized with $NH_2$, (c) PANI functionalized with OH in the presence of $NH_3$.

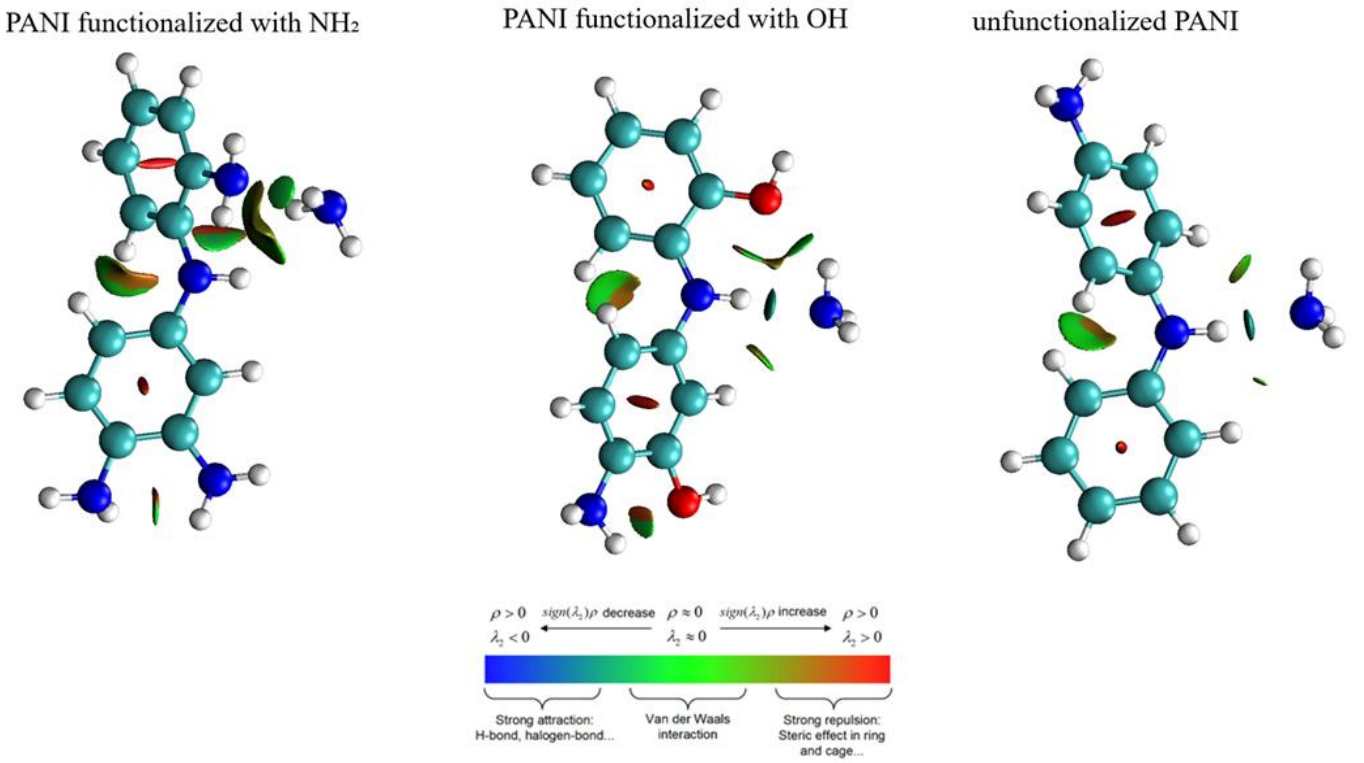


**Fig. 6:** Non-covalent interactions of PANI functionalized with $NH_2$, PANI functionalized with OH, and unfunctionalized PANI in the presence of $NH_3$. Color key: white (H atom); grey (C atom); blue (N atom); red (O atom).

### 3.6 Critical points

Fig. 7 displays the critical points derived from the topological analysis of the electron density for $NH_2$-functionalized PANI, OH-functionalized PANI, and unfunctionalized PANI, each complexed with adsorbed $NH_3$ Critical points are specific points in the electron density scalar field where the gradient of the electron density is zero. In the context of molecular interactions, bond critical points (BCPs), often depicted as small yellow spheres, are particularly important as they signify a bond path and provide evidence of an interaction between two atoms. The presence and characteristics of these BCPs offer quantitative insights into the nature and strength of intermolecular interactions, such as hydrogen bonds or other non-covalent interactions.

For the $NH_2$-functionalized PANI system with adsorbed ammonia, Fig. 7 clearly shows several bond critical points (yellow spheres) located along the lines connecting the hydrogen atoms of the ammonia molecule to the nitrogen atoms of the PANI backbone and the amino functional group. The existence of these BCPs, along with the bond paths (orange lines connecting atoms via the BCPs), provides definitive topological evidence of hydrogen bonding interactions between the $NH_3$ molecule and the functionalized PANI. The multiplicity and location of these BCPs indicate strong, direct, and specific interactions that facilitate the stable adsorption of $NH_3$. The amino group appears to act as a key site for these interactions, drawing the $NH_3$ molecule into a favorable binding configuration between the $NH_3$ and the hydroxyl group, or other parts of the PANI structure. While some interaction is evident, it appears to be less extensive or as strongly defined compared to the $NH_2$-functionalized PANI. This suggests that the hydrogen bonding capabilities of the hydroxyl group with $NH_3$ might be weaker or less optimized than those of the amino group. For the unfunctionalized PANI, the critical points between the $NH_3$ and the PANI backbone are even more sparse and less pronounced, primarily indicating very weak or non-specific interactions, likely limited to van der Waals forces. The absence of strong, well-defined BCPs between $NH_3$ and unfunctionalized PANI suggests a lack of specific binding sites.

The topological analysis via critical points in Fig. 7 strongly reinforces the conclusions drawn from the MEP maps and Mulliken charges. The clear presence of multiple, well-defined bond critical points signifying hydrogen bonds in the $NH_2$-functionalized PANI system provides robust evidence for its superior ability to interact strongly and specifically with $NH_3$. This direct evidence of bond formation and interaction pathways confirms that the $NH_2$ functionalization creates highly effective binding sites, thereby enhancing the overall $NH_3$ sensing performance, aligning perfectly with our hypothesis.

### 3.7 Molecular orbitals

Our working hypothesis suggests that the sensitivity of PANI derivatives to ammonia follows the trend: $NH_2$ functionalized PANI > OH-functionalized PANI > unfunctionalized PANI.

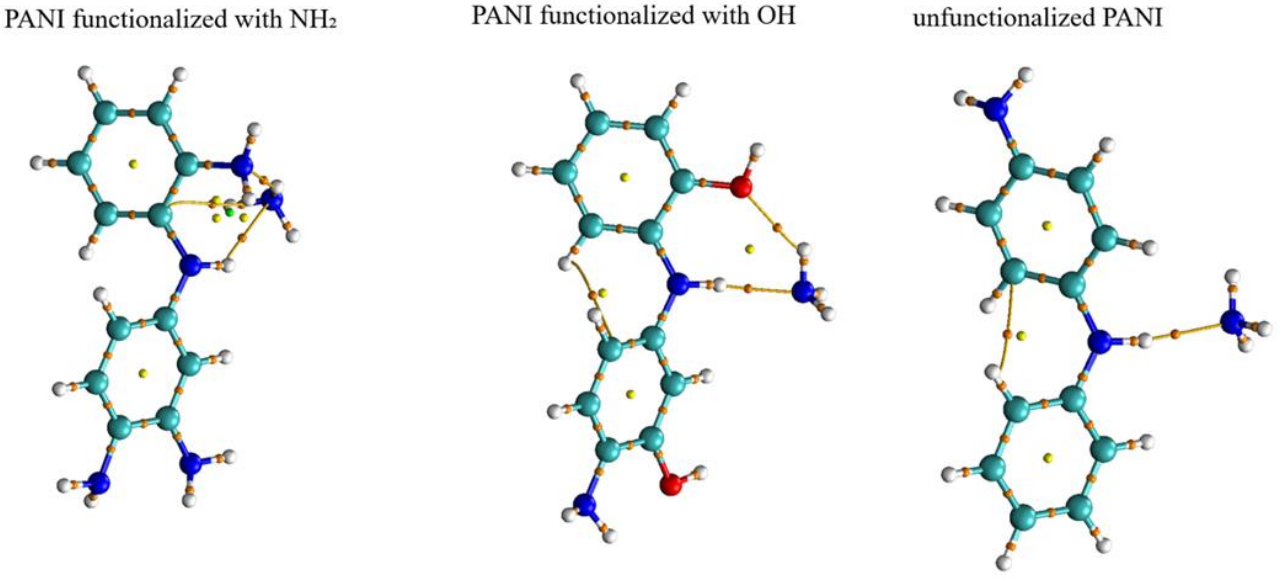


**Fig. 7:** Critical points of PANI functionalized with $NH_2$, PANI functionalized with OH, and unfunctionalized PANI in the presence of $NH_3$. Color key: white (H atom); grey (C atom); blue (N atom); red (O atom).

This is based on the rationale that functional groups can significantly influence the electronic environment of PANI and, by extension, its interaction strength with $NH_3$, a Lewis base that donates electrons upon adsorption. To explore this, we performed a comparative frontier molecular orbital analysis, focusing on the Highest Occupied Molecular Orbital (HOMO) and Lowest Unoccupied Molecular Orbital (LUMO) of the PANI– $NH_3$ complexes. As shown in Fig. 8, $NH_2$-functionalized PANI exhibits a LUMO localized near the $NH_3$ molecule and the amine functional site, indicating strong orbital overlap and a favorable electron-accepting interaction. This localization facilitates enhanced charge transfer or hydrogen bonding between $NH_3$ and the polymer, potentially amplifying sensor response.

Interestingly, despite $NH_2$-functionalized PANI exhibiting the largest HOMO-LUMO energy gap (4.48 eV) compared to OH-functionalized (3.94 eV) and unfunctionalized PANI (3.95 eV), the specific orbital alignment and localization appear more critical than the gap magnitude alone. While OH- and unfunctionalized PANI systems have slightly smaller gaps and higher HOMO energies, indicating relatively easier oxidation, their molecular orbitals are less directly involved in $NH_3$ interactions, suggesting weaker perturbation upon adsorption. The OH group, although capable of forming hydrogen bonds, provides a less effective electronic coupling site than the $NH_2$ group, which is more basic and spatially accessible.

Thus, the orbital distribution analysis supports our hypothesis that $NH_2$-functionalized PANI offers a more favorable binding site for $NH_3$, enhancing sensitivity through stronger electronic interactions. This highlights the importance of not just energy gap metrics, but also orbital spatial characteristics in designing effective functionalized polymer-based gas sensors.

### 3.8 Molecular structures

Fig. 9 displays the temporal evolution of the molecular structures of unfunctionalized and functionalized PANI systems during the production phase of the classical all-atom MD simulation. The figure captures the dynamic behavior of PANI chains in the presence of $NH_3$ (shown in red) and air molecules (represented in green with transparency), offering insights into how chemical modifications influence PANI's morphology and interaction dynamics.

The top row illustrates unfunctionalized PANI, which retains a relatively compact structure throughout the simulation. The polymer chains exhibit modest configurational rearrangements, indicative of their stable but less interactive nature. In this native form, PANI's conductivity arises from its conjugated backbone, but its interaction with surrounding molecules like $NH_3$ is limited due to the absence of polar functional sites.

The middle row shows $NH_2$-functionalized PANI. The presence of amine groups introduces local polarity and hydrogen bonding capabilities, enhancing the polymer's ability to interact with polar molecules. Over time, the $NH_2$-functionalized chains exhibit increased spatial extension and moderate swelling, suggesting that the incorporation of $NH_2$ facilitates better dispersion and stronger interactions with $NH_3$ molecules. These interactions are primarily driven by hydrogen bonding and acid-base attractions, which can modulate the polymer's electronic properties. The bottom row depicts OH-functionalized PANI, where hydroxyl groups add further polarity and enable extensive hydrogen bonding with $NH_3$ and water vapor from the surrounding air. Compared to the other systems, the OH-functionalized PANI chains appear more relaxed and dispersed, reflecting higher solvation and intermolecular interaction. The structural openness likely enhances the accessibility of $NH_3$ to the polymer backbone, making it particularly suitable for sensing applications.

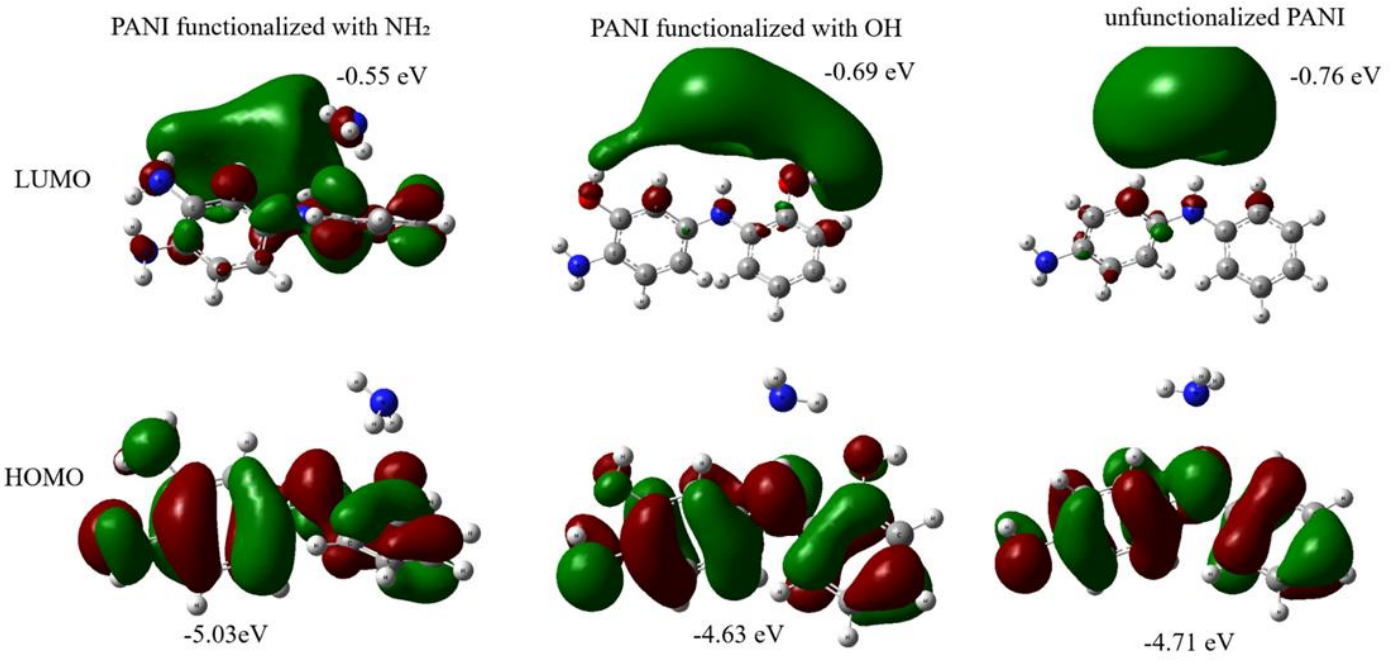


**Fig. 8:** Molecular orbitals of PANI functionalized with $NH_2$, PANI functionalized with OH, and unfunctionalized PANI in the presence of $NH_3$. Color key: white (H atom); grey (C atom); blue (N atom); red (O atom).

Herein, functionalization significantly affects the dynamic architecture of PANI. The introduction of $NH_2$ and OH groups enhances the polymer's interaction with $NH_3$, which is critical for sensing mechanisms that rely on conductivity modulation. These findings underscore the importance of molecular-level design in tuning PANI's structure–property relationships for targeted sensor performance.

### 3.9 Radial distribution function

Fig. 10 presents the radial distribution function (RDF) analysis to investigate intermolecular interactions in different PANI systems. Subfigure (a) shows the RDF between nitrogen atoms of PANI chains (PANI/PANI), while subfigure (b) illustrates the RDF between nitrogen atoms of PANI and hydrogen atoms of $NH_3$, indicating the extent of interaction between PANI (or functionalized PANI) and $NH_3$.

In Fig. 10a, all three systems, unfunctionalized PANI, $NH_2$-functionalized PANI, and OH-functionalized PANI which is exhibiting sharp and intense RDF peaks around ~5.8 Å. This peak suggests a characteristic interchain nitrogen-nitrogen distance maintained across systems, pointing to consistent structural packing. Notably, the similarity in peak positions and heights among the systems indicates that functionalization does not significantly disrupt the intrinsic PANI chain-chain interactions.

However, in Fig. 10b, significant differences arise in RDF profiles for PANI-$NH_3$ interactions. $NH_2$-functionalized PANI shows the highest and most distinct RDF peak at ~3.3 Å, indicating strong and well-defined interactions with $NH_3$ via hydrogen bonding. This aligns with the chemical nature of $NH_2$, which readily forms hydrogen bonds with $NH_3$'s hydrogen atoms. OH-functionalized PANI also shows a strong peak but at slightly longer distances, consistent with its role primarily as a hydrogen bond donor. In contrast, unfunctionalized PANI displays broader and lower-intensity peaks, suggesting weaker and more dispersed interactions with $NH_3$ molecules.

The order of RDF peak intensity and proximity is as follow: $NH_2$-functionalized > OH-functionalized > unfunctionalized which is correlating well with the observed number of hydrogen bonds and supports the hypothesis that $NH_3$ sensitivity is enhanced by polar functional groups. These findings underline the role of functional groups in tuning the local structure and interaction strength, which is essential for optimizing PANI-based $NH_3$ sensing materials.

### 3.10 Number of hydrogen bonds

Table 3 presents the number of hydrogen bonds formed between variously functionalized PANI systems and $NH_3$ molecules

The results reveal a clear trend consistent with the hypothesized $NH_3$ sensitivity: $NH_2$-functionalized PANI exhibits the highest number of hydrogen bonds (25), followed by OH-functionalized PANI (23), and finally unfunctionalized PANI (20). This increase in hydrogen bonding capacity can be attributed to the nature of the introduced functional groups. The $NH_2$ group, capable of acting as both hydrogen bond donor and acceptor, provides the most versatile and favorable interaction sites for $NH_3$ molecules. The OH group, while also enabling hydrogen bonding, primarily serves as a donor, slightly limiting the interaction flexibility compared to $NH_2$. In contrast, unfunctionalized PANI lacks specific polar

functional groups, resulting in weaker and less frequent interactions with $NH_3$. These findings support the predicted sensitivity order, where stronger and more numerous hydrogen bonds facilitate more robust interactions between PANI and ammonia, potentially enhancing the sensing response through changes in the local electronic environment or polymer conductivity. Overall, the H-bond analysis strengthens the molecular-level understanding of how functional group modification improves ammonia sensing in PANI-based materials.

### 3.11 Comparison of our work with experiment

The simulated trend ($NH_2$-PANI > OH-PANI >. unfunctionalized PANI) aligns with experimental systems

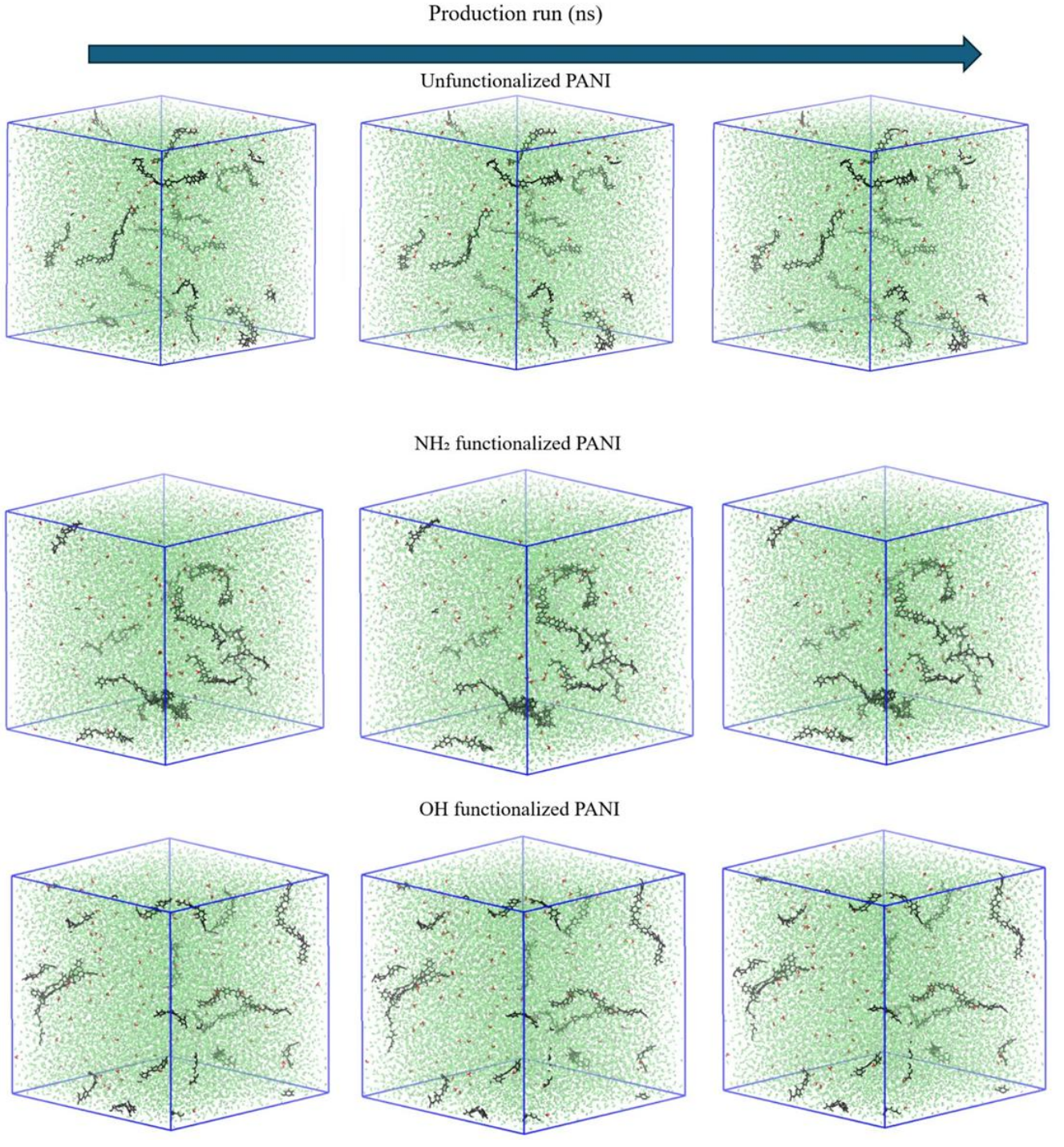


**Fig. 9:** Molecular structures of unfunctionalized PANI (dynamic bond, black), PANI (dynamic bond, black) functionalized with $NH_2$, PANI (dynamic bond, black) functionalized with OH in the presence of $NH_3$ (dynamic bond, red) and air (dynamic bond, green, transparent).

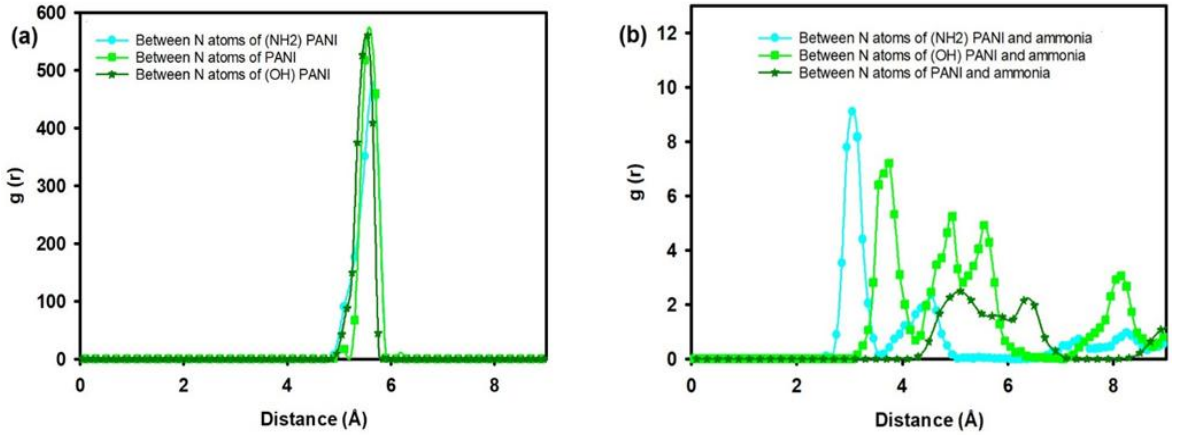


**Fig. 10:** RDFs for (a) between nitrogen atoms of PANI/PANI, (b) between nitrogen atoms of PANI and hydrogen atoms of ammonia.

**Table 3:** Number of hydrogen bonds for PANI with ammonia.

| | Number of hydrogen bonds |
|---|---|
| Unfunctionalized PANI with ammonia | 20 |
| $NH_3$ functionalized PANI with ammonia | 25 |
| OH functionalized PANI with ammonia | 23 |

employing functional groups or nanostructured composites. For instance, the SDS-functionalized PANI sensor achieves a remarkable 0.1 ppm detection limit and 12 s recovery time, consistent with our finding that targeted functionalization (-$NH_2$/-OH) strengthens $NH_3$ interactions through hydrogen bonding and charge redistribution (Table 4). Similarly, the rGO-PANI composite leverages carboxylic acid groups on rGO to enhance protonation kinetics (Table 4), mirroring the role of -$NH_2$/-OH groups in our simulations. However, the PANI/$TiO_2$ system demonstrates that heterostructure engineering (rather than chemical functionalization) can also achieve high sensitivity (5.4 at 100 ppm) (Table 4), suggesting combined approaches might yield optimal performance. Notably, all high-performing experimental systems exceed the baseline unfunctionalized PANI in both sensitivity and detection limit, validating the computational prediction that intentional modifications (chemical or structural) are critical for advanced $NH_3$ sensing. These comparisons underscore the practical relevance of tailoring PANI's electronic and steric properties through functionalization, as demonstrated in our simulations.

In the conducting emeraldine salt (ES) state, PANI contains protonated imine nitrogen atoms ($N^+$–H) which act as primary adsorption sites for electron-donating gases like ammonia. Upon exposure to $NH_3$, these $N^+$–H sites undergo a reversible deprotonation, transforming ES into the semiconducting emeraldine base (EB) form, accompanied by the formation of $NH_4^+$ and the release of electrons into the PANI backbone. Functionalization with $NH_2$ or OH groups modifies the local electronic environment of the polymer, potentially influencing this process. The $NH_2$ group, being a strong electron-donating group, increases the local electron density around adjacent nitrogen atoms, which can stabilize the $N^+$–H site and modulate its deprotonation energy. This effect can facilitate more efficient electron injection when $NH_3$ interacts with the site, enhancing the sensor response. In contrast, the OH group also engages in electron-donating effect. As a result, while it can still support $NH_3$ interaction via secondary hydrogen bonding, its influence on the deprotonation of $N^+$–H sites is less pronounced than $NH_2$. Our simulation data—supported by interaction energy and hydrogen bond analysis—indicate that

**Table 4:** Comparison of our work with experimental PANI based $NH_3$ sensors.

| Composite | Detection limit | Sensitivity | Response/Recovery time | Key findings |
|---|---|---|---|---|
| rGO-PANI composite.[40] | 5 ppm | ~3.0 slope (5-100 ppm) | 97 s / 680 s | Synergistic protonation between rGO and PANI |
| SDS-functionalized PANI.[41] | 0.1 ppm | 5.4 (40 ppm) | 12 s recovery | Ordered PANI chains from SDS templating |
| PANI-MWCNTs/PDMS.[42] | 10 ppb | 11.8 (40 ppm) | 236 s recovery | High surface area from MWCNTs/PANI hybrid |
| PANI/$TiO_2$ nanocomposite.[43] | 0.5 ppm | 5.4 (100 ppm) | 100 s / 232 s | p-n heterojunction enhances charge transfer |

$NH_2$-functionalized PANI promotes a more favorable environment for ammonia-induced electron transfer due to stronger stabilization of transition states and intermediates, which aligns with experimental observations of enhanced sensing performance.

## 4. Conclusion

This computational study aimed to elucidate the ammonia ($NH_3$) sensing mechanisms of polyaniline (PANI) and its functionalized derivatives using a multiscale simulation approach. Density Functional Theory (DFT) calculations and Molecular Dynamics (MD) simulations were employed to analyze the structural, electronic, and interaction-level behaviors of unfunctionalized, $NH_2$-functionalized, and OH-functionalized PANI in the presence of $NH_3$ and ambient conditions. The goal was to understand how chemical modifications influence $NH_3$ sensing performance and to identify which functionalization confers the greatest sensitivity.

The DFT analysis revealed that functionalization with $NH_2$ and OH groups enhances the electron density and charge localization at the sites of modification, as shown through Molecular Electrostatic Potential (MEP) maps and Mulliken charge distributions. Reduced Density Gradient (RDG) and Non-Covalent Interaction (NCI) analyses demonstrated that $NH_2$-functionalized PANI engages in the most substantial hydrogen bonding and van der Waals interactions with $NH_3$. The Quantum Theory of Atoms in Molecules (QTAIM) confirmed the presence of additional bond critical points in the $NH_2$-functionalized system, indicating stronger and more numerous interactions. Moreover, interaction energy calculations showed that $NH_2$-functionalized PANI has the most negative binding energy with $NH_3$, highlighting its superior affinity and stability.

MD simulations provided further insight into the dynamic behavior of PANI and its derivatives in the presence of $NH_3$ and air. The visual snapshots showed that functionalized PANI, especially the $NH_2$ variant, exhibited more significant conformational changes upon $NH_3$ exposure, which is consistent with enhanced interaction strength and suggests potential for greater conductivity modulation. These dynamic alterations support the proposed sensitivity trend: $NH_2$-functionalized PANI > OH-functionalized PANI > unfunctionalized PANI.

In conclusion, this integrated DFT and MD study convincingly demonstrates that chemical functionalization of PANI, especially with $NH_2$ groups, significantly enhances its $NH_3$ sensing performance by improving interaction strength and structural adaptability. These theoretical insights offer valuable design guidelines for developing next-generation PANI-based gas sensors; however, further experimental validation, coupled with real-environment simulations, remains crucial to confirm long-term stability, assess cross-sensitivity, and ensure scalability. Looking ahead, our future work will explore other functional groups or copolymer systems for selective detection of a broader range of gases pertinent to environmental monitoring and healthcare applications. We also aim to extend this study by performing time-dependent DFT calculations to investigate the optical properties and excitation behavior of functionalized PANI systems upon ammonia adsorption, thereby assessing their potential for optical sensing, and plan to investigate the impact of varying humidity levels on ammonia sensing using extended classical MD simulations to better replicate real-world environmental conditions. Additionally, we intend to conduct concentration-dependent simulations to evaluate the sensitivity of functionalized PANI across a wider range of $NH_3$ levels, from trace to elevated concentrations, and perform comprehensive Natural Bond Orbital (NBO) analysis to quantitatively assess charge transfer, orbital interactions, and electronic stabilization in the ammonia complexes with functionalized PANI.

## Acknowledgments

This research was funded by the Science Committee of the Ministry of Science and Higher Education of the Republic of Kazakhstan (Grant No. AP19175789).

## Conflict of Interest

The authors declare no conflict of interest.

## Supporting Information

Not applicable.

## CRediT Statement

**Areyi Nulimu:** Data curation, Data visualization, Formal analysis, Methodology, Writing – original draft. **Anuar Aldongarov:** Resources, Writing – review & editing. **Saniya Sarsenova:** Data curation, Validation, Writing – review & editing. **Aigerim Ibrayeva:** Supervision, Funding acquisition, Writing – review & editing. **Mirat Karibayev:** Conceptualization, Supervision, Writing – review & editing.

## References

[1] S. Mingolla, P. Gabrielli, A. Manzotti, M. J. Robson, K. Rouwenhorst, F. Ciucci, G. Sansavini, M. M. Klemun, Z. Lu, Effects of emissions caps on the costs and feasibility of low-carbon hydrogen in the European ammonia industry, *Nature Communications*, 2024, **15**, 3753, doi: 10.1038/s41467-024-48145-z.

[2] D. Shah, M. Karibayev, E. K. Adotey, M. Amouei Torkmahalleh, Impact of volatile organic compounds on chromium containing atmospheric particulate: insights from molecular dynamics simulations, *Scientific Reports,* 2020, **10**, 17387, doi: 10.1038/s41598-020-74522-x..

[3] W. Lv; J. Yang; Q. Xu; J. A.-A. Mehrez; J. Shi; W. Quan; H. Luo; M. Zeng; N. Hu; T. Wang; H. Wei; Z. Yang, Wide-range and high-accuracy wireless sensor with self-humidity compensation

for real-time ammonia monitoring, *Nature Communications*, 2024, **15**(1), doi: 10.1038/s41467-024-51279-9.
[4] T. Zhang; W. Li; Y. Shi; C. Li, Polyaniline-based room temperature ammonia gas sensor employing hybrid organic-inorganic substrate, *Materials Chemistry and Physics*, 2022, **288**, 126404, doi: 10.1016/j.matchemphys.2022.126404.
[5] T. N. Ly; S. Park, Highly sensitive ammonia sensor for diagnostic purpose using reduced graphene oxide and conductive polymer, *Scientific Reports*, 2018, **8**(1), doi: 10.1038/s41598-018-36468-z.
[6] M. Amouei Torkmahalleh, M. Karibayev, D. Konakbayeva, M. M. Fyrillas, A. M. Rule, Aqueous chemistry of airborne hexavalent chromium during sampling, *Air Quality, Atmosphere & Health*, 2018, **11**, 1059-1068, doi: 10.1007/s11869-018-0607 z
[7] L. Yang; X. Xu; M. Liu; C. Chen; J. Cui; X. Chen; K. Wu; D. Sun, Wearable and flexible bacterial cellulose/polyaniline ammonia sensor based on a synergistic doping strategy, *Sensors and Actuators B: Chemical*, 2021, **334**, 129647, doi: 10.1016/j.snb.2021.129647.
[8] S. Mikhaylov; N. A. Ogurtsov; N. Redon; P. Coddeville; J.-L. Wojkiewicz; A. A. Pud, The PANI-DBSA content and dispersing solvent as influencing parameters in sensing performances of $TiO_2$/PANI-DBSA hybrid nanocomposites to ammonia, *RSC Advances*, 2016, **6**(86), 82625–82634, doi: 10.1039/c6ra12693f.
[9] T. Das; S. Mojumder; D. Saha; M. Pal, Enhanced ammonia sensing performance of barium hexaferrite enabled through Zn doping: Mechanistic study considering modulation of $Fe^{2+}/Fe^{3+}$ ratio and oxygen vacancy, *Sensors and Actuators B: Chemical*, 2024, **406**, 135358, doi: 10.1016/j.snb.2024.135358.
[10] M. B. Kumbhar; V. S. Chandak; P. M. Kulal, Enhanced ammonia gas sensing performance at room temperature of binder-free NiO, Cu and Co-doped NiO thin films synthesized via the SILAR method, *Materials Chemistry and Physics*, 2025, **329**, 130065, doi: 10.1016/j.matchemphys.2024.130065.
[11] P. Askar, D. Kanzhigitova, A. Ospanova, A. Tapkharov, S. Duisenbekov, M. Abutalip, B. Soltabayev, A. Turlybekuly, S. Adilov, N. Nuraje, 1 ppm-detectable hydrogen gas sensor based on nanostructured polyaniline, *Scientific Reports*, 2024, **14**, 26984, doi: 10.1038/s41598-024-77083-5.
[12] R. J. Rath, S. Talebian, J. Giaretta, S. Naficy, F. Dehghani, Organic-based chemiresistive sensors for detection of water-soluble gases: strategies and roadmap for enhancing sensing performance, *Advanced Functional Materials*, 2025, **35**, 2417323, doi: 10.1002/adfm.202417323.
[13] M. Hjiri, S. Algessair, R. Dhahri, H. B. Albargi, N. Ben Mansour, A. A. Assadi, G. Neri, Ammonia gas sensors based on undoped and Ca-doped ZnO nanoparticles, *RSC Advances*, 2024, **14**(8), 5001-5011, doi: 10.1039/d3ra08181h.
[14] M. Karibayev, D. Shah, Comprehensive computational analysis exploring the formation of caprolactam-based deep eutectic solvents and their applications in natural gas desulfurization, *Energy & Fuels*, 2020, **34**, 9894-9902, doi: 10.1021/acs.energyfuels.0c01721.
[15] J. Li, S. Dong, Y. Duan, X. Fu, G. Li, Y. Huang, Polyaniline composited with rGO wrapped-$SiO_2$ microsphere ammonia sensor with fast response/recovery and high sensitivity for pig healthy breeding, *Sensors and Actuators B: Chemical*, 2024, **398**, 134784, doi: 10.1016/j.snb.2023.134784.
[16] S. D. Lawaniya, S. Kumar, Y. Yu, K. Awasthi, Nitrogen-doped carbon nano-Onions/polypyrrole nanocomposite based low-cost flexible sensor for room temperature ammonia detection, *Scientific Reports*, 2024, **14**(1), 7904, doi: 10.1038/s41598-024-57153-4.
[17] P. Pradeep Kumar, V. Singh, Enhanced dual gas sensing performance of $MoS_2/MoO_3$ nanostructures for $NH_3$ and $NO_2$ detection, *Ceramics International*, 2024, **50**, 21978-21988, doi: 10.1016/j.ceramint.2024.03.312.
[18] J. Liang, D. Hu, W. Xu, L. Peng, K. Liu, Y. Fang, Interfacially confined dynamic reaction resulted to fluorescent nanofilms depicting high-performance ammonia sensing, *Analytical Chemistry*, 2024, **96**(5), 2152-2157, doi: 10.1021/acs.analchem.3c05032.[PubMed]
[19] X. Li, W. Zeng, S. Zhuo, B. Qian, Q. Chen, Q. Luo, R. Qian, Highly sensitive room-temperature detection of ammonia in the breath of kidney disease patients using $Fe_2Mo_3O_8/MoO_2$@$MoS_2$ nanocomposite gas sensor, *Advanced Science*, 2024, **11**, 2405942, doi: 10.1002/advs.202405942.
[20] A. Maity, S. Mitra, B. Ghosh, Textile based lead-free halide perovskite $CH_3NH_3SnI_3$ ammonia gas sensor working at room temperature, *ACS Applied Electronic Materials*, 2024, **6**, 2677-2682, doi: 10.1021/acsaelm.4c00230.
[21] Z. Pang, E. Yildirim, M. A. Pasquinelli, Q. Wei, Ammonia sensing performance of polyaniline-coated polyamide 6 nanofibers, *ACS Omega*, 2021, **6**(13), 8950-8957, doi: 10.1021/acsomega.0c06272.
[22] B. Li, Y. Li, P. Ma, Synthesis of different inorganic acids doped polyaniline materials and behavior of enhancing $NH_3$ gas sensing properties, *Organic Electronics*, 2023, **114**, 106749, doi: 10.1016/j.orgel.2023.106749.
[23] H. Ullah, A.-U.-H. Ali Shah, S. Bilal, K. Ayub, DFT study of polyaniline $NH_3$, $CO_2$, and CO gas sensors: comparison with recent experimental data, *The Journal of Physical Chemistry C*, 2013, **117**, 23701-23711, doi: 10.1021/jp407132c.
[24] A. Verma, T. Kumar, Ag/Cu doped polyaniline hybrid nanocomposite-based novel gas sensor for enhanced ammonia gas sensing performance at room temperature, *RSC Advances*, 2024, **14**, 25093-25107, doi: 10.1039/D4RA04009K.
[25] H. Zhang, X. Zhang, C. Qiu, P. Jia, F. An, L. Zhou, L. Zhu, D. Zhang, Polyaniline/ZnO heterostructure-based ammonia sensor self-powered by electrospinning of PTFE-PVDF/MXene piezo-tribo hybrid nanogenerator, *Chemical Engineering Journal*, 2024, **496**, 154226, doi: 10.1016/j.cej.2024.154226.
[26] P. M. W. Gill, B. G. Johnson, J. A. Pople, M. J. Frisch, The performance of the becke: lee: Yang: parr (B: LYP) density functional theory with various basis sets, *Chemical Physics Letters*, 1992, **197**, 499-505, doi: 10.1016/0009-2614(92)85807-M.
[27] E. V. R. de Castro, F. E. Jorge, Accurate universal Gaussian basis set for all atoms of the Periodic Table, *The Journal of Chemical Physics*, 1998, **108**, 5225-5229, doi: 10.1063/1.475959.

[28] Gaussian 16, Revision C.01, M. J. Frisch, G. W. Trucks, H. B. Schlegel, G. E. Scuseria, M. A. Robb, J. R. Cheeseman, *et al.* (2016). *Gaussian, Inc.,* Wallingford CT.
[29] GaussView, Version 6, Dennington, R., Keith, T. A., & Millam, J. M. (2016). *Semichem Inc*., Shawnee Mission, KS.
[30] T. Lu, F. Chen, Multiwfn: a multifunctional wavefunction analyzer, *Journal of Computational Chemistry*, 2012, **33**(5), 580-592, doi: 10.1002/jcc.22885.
[31] N. Kydyrbay, M. Zhazitov, M. Abdullah, T. Duisebayev, Y. Tezekbay, A. Aldongarov, M. Karibayev, N. Nuraje, O. Toktarbaiuly, Structural, surface, and theoretical investigation of hydrophobic-modified nanodiamond powders, *Scientific Reports*, 2025, **15**, 24329, doi: 10.1038/s41598-025-10027-9.
[32] W. Humphrey, A. Dalke, K. Schulten, VMD: visual molecular dynamics, *Journal of Molecular Graphics*, 1996, **14**(1), 33-38, 27-28, doi: 10.1016/0263-7855(96)00018-5.
[33] A. K. Malde, L. Zuo, M. Breeze, M. Stroet, D. Poger, P. C. Nair, C. Oostenbrink, A. E. Mark, An automated force field topology builder (ATB) and repository: version 1.0, *Journal of Chemical Theory and Computation*, 2011, **7**, 4026-4037, doi: 10.1021/ct200196m.
[34] N. Schmid, A. P. Eichenberger, A. Choutko, S. Riniker, M. Winger, A. E. Mark, W. F. van Gunsteren, Definition and testing of the GROMOS force-field versions 54A7 and 54B7, *European Biophysics Journal*, 2011, **40**(7), 843-856, doi: 10.1007/s00249-011-0700-9.
[35] P. P. Ewald, Die berechnung optischer und elektrostatischer gitterpotentiale, *Annalen der Physik*, 1921, **369**, 253-287, doi: 10.1002/andp.19213690304.
[36] D. J. Evans, B. L. Holian, The nose–hoover thermostat, *The Journal of Chemical Physics*, 1985, **83**, 4069-4074, doi: 10.1063/1.449071.
[37] H. J. C. Berendsen, Transport properties computed by linear response through weak coupling to a bath. *Computer Simulation in Materials Science*. Dordrecht: Springer Netherlands, 1991, 139-155, doi: 10.1007/978-94-011-3546-7_7.
[38] D. Van Der Spoel, E. Lindahl, B. Hess, G. Groenhof, A. E. Mark, H. J. Berendsen, GROMACS: fast, flexible, and free, *Journal of Computational Chemistry*, 2005, **26**(16), 1701-1718, doi: 10.1002/jcc.20291.
[39] R. Floors, M. Nielsen, Estimating air density using observations and re-analysis outputs for wind energy purposes, *Energies*, 2019, **12**, 2038, doi: 10.3390/en12112038.
[40] F. S. Hadano, A. E. X. Gavim, J. C. Stefanelo, S. L. Gusso, A. G. Macedo, P. C. Rodrigues, A. R. B. Mohd Yusoff, F. K. Schneider, J. F. Deus, W. José da Silva, $NH_3$ sensor based on rGO-PANI composite with improved sensitivity, *Sensors*, 2021, **21**(15), 4947, doi: 10.3390/s21154947.
[41] C. Zhu, Y. Xu, T. Zhou, L. Liu, Q. Chen, B. Gao, T. Zhang, Self-assembly polyaniline films for the high-performance ammonia gas sensor, *Sensors and Actuators B*: *Chemical*, 2022, **365**, 131928, doi: 10.1016/j.snb.2022.131928.
[42] C. Zhu, T. Zhou, H. Xia, T. Zhang, Flexible room-temperature ammonia gas sensors based on PANI-MWCNTs/PDMS film for breathing analysis and food safety, *Nanomaterials*, 2023, **13**, 1158, doi: 10.3390/nano13071158.
[43] C, Zhu, X. Cheng, X. Dong, Y. Xu, Enhanced sub-ppm $NH_3$ gas sensing performance of PANI/$TiO_2$ nanocomposites at room temperature. *Frontiers in Chemistry,* 2018, **6**, 493-503, doi:10.3389/fchem.2018.00493.